nature climate change

SUPPLEMENTARY INFORMATION

DOI: 10.1038/NCLIMATE2580

# Mineral protection of soil carbon counteracted by root exudates

*Marco Keiluweit*[1,2*], *Jeremy J. Bougoure*[2,3], *Peter S. Nico*[4], *Jennifer Pett-Ridge*[2], *Peter K. Weber*[2] and *Markus Kleber*[1,5]

[1] Department of Crop and Soil Science, Oregon State University, ALS Building 3017, Corvallis, OR-97331, USA

[2] Chemical Sciences Division, Lawrence Livermore National Laboratory, 7000 East Ave, L-231, Livermore, CA-94550, USA

[3] School of Earth & Environment, University of Western Australia, 35 Stirling Hwy, Crawley. 6009, Australia

[4] Earth Sciences Division, Lawrence Berkeley National Laboratory, 1 Cyclotron Rd, Berkeley, CA-94720, USA

[5] Leibnitz-Zentrum fur Agrarlandschaftsforschung (ZALF) e.V. Eberswalder Straβe 84, 15374 Müncheberg, Germany

[*]Corresponding author address:
Marco Keilweit
Stockbridge School of Agriculture
University of Massachusetts—Amherst
411 Paige Laboratory
Amherst, MA-01003, USA
Email: keiluweit@umass.edu

# Table of content

## 1. Tables

**Table S-1: Physical-chemical properties of soils used in this study**

| | **Grassland soil** | **Forest soil** |
|---|---|---|
| Classification (U.S. taxonomy) | Typic Haploxeroll | Humic Dystrudept |
| Texture | silty-loam | clay loam |
| Horizon and sampling depth | $A_p$ (0-10 cm) | $A_h$ (0-20 cm) |
| Bulk density (g $cm^{-3}$) | 1.24 | 1.04 |
| Field capacity* (%) | 20% | 32% |
| pH# | 5.3 | 4.8 |
| $C_{org}$ (%) | 1.4 | 1.5 |
| C/N | | |
| $NO_3^-$-N (ppm) | 23 | 0.3 |
| $NH_4^+$-N (ppm) | 1.5 | 5.5 |
| Bray-P (ppm) | 53 | 4 |
| CEC (meq $kg^{-1}$) | 13.6 | 12.7 |
| Soluble salts (Ms $cm^{-1}$) | 0.56 | 0.05 |
| Carbonate | n.d. | n.d. |

* soil moisture retained at -0.33 bar hydraulic head as percentage of dry weight
# in 0.01M $CaCl_2$

**Table S-2: Fit parameters for oxygen diffusion model in a cylindrical system presented in Fig. 1b**

| Soil | Treatment | Fit equation‡ | $R^2$ |
|---|---|---|---|
| Silt loam | Glucose | C(r) = 32 ln(r) + 152 | 0.90 |
| | Oxalic acid | C(r) = 48 ln(r) + 94 | 0.92 |
| | Acetic acid | C(r) = 15 ln(r) + 186 | 0.95 |
| Clay | Glucose | C(r) = 9 ln(r) + 187 | 0.97 |
| | Oxalic acid | C(r) = 23 ln(r) + 151 | 0.98 |
| | Acetic acid | C(r) = 10 ln(r) + 181 | 0.86 |

64

**Table S-3: Summary of the sequential extraction procedure***

| Step | Metal phases (Fe, Al, Si, Mn, Ca) | Extraction |
|---|---|---|
| 1 | Organically complexed | 40 mL 0.2M Na-pyrophosphate at pH 10, agitated for 4 h‡, centrifuged§, rinsed¶ |
| 2 | Acid-soluble | 40 mL 1M ammonium acetate at pH 3.0, agitated for 4 h‡, centrifuged§, rinsed¶ |
| 3 | Poorly-crystalline, short-range order | 40 mL 0.2M ammonium oxalate at pH 3, agitated for 4 h‡, centrifuged§, rinsed¶ |

‡ on reciprocal shaker at 100 rounds per minute
§ centrifuged for 15 min at 900 x g
¶ rinsed twice with MilliQ $H_2O$

65
66

**Table S-4: Extractable metal concentrations in root, intermediate and bulk zones in silt loam (mean ± standard deviation, n = 2)**

| Extractant | Treatment | Distance | Al | Si | Mn | Ca | Fe |
|---|---|---|---|---|---|---|---|
| | | mm | | | $\mu$mol g$^{-1}$ | | |
| Na-PP | Glucose | 0-4 | 16 ± 1 | 12 ± 0 | 1.7 ± 0.3 | 64 ± 0 | 11 ± 0 |
| (pH = 10) | | 4-12 | 16 ± 0 | 13 ± 0 | 1.1 ± 0.0 | 63 ± 3 | 11 ± 0 |
| | | 13-50 | 17 ± 2 | 14 ± 0 | 1.1 ± 0.0 | 65 ± 2 | 10 ± 0 |
| | Oxalic acid | 0-4 | 4 ± 0 | 8 ± 1 | 1.2 ± 0.1 | 79 ± 11 | 4 ± 0 |
| | | 4-12 | 8 ± 1 | 10 ± 0 | 1.5 ± 0.0 | 64 ± 3 | 6 ± 0 |
| | | 13-50 | 19 ± 1 | 17 ± 1 | 1.0 ± 0.1 | 65 ± 2 | 11 ± 1 |
| | Acetic acid | 0-4 | 8 ± 4 | 11 ± 1 | 0.6 ± 0.1 | 60 ± 2 | 7 ± 3 |
| | | 4-12 | 16 ± 0 | 13 ± 1 | 1.0 ± 0.1 | 64 ± 1 | 11 ± 0 |
| | | 13-50 | 18 ± 2 | 13 ± 0 | 1.1 ± 0.1 | 67 ± 3 | 11 ± 0 |
| | Control | 0-4 | 20 ± 1 | 19 ± 3 | 1.1 ± 0.1 | 66 ± 2 | 12 ± 1 |
| | | 4-12 | 18 ± 1 | 15 ± 0 | 1.1 ± 0.1 | 66 ± 2 | 11 ± 0 |
| | | 13-50 | 18 ± 1 | 15 ± 1 | 1.1 ± 0.1 | 67 ± 3 | 11 ± 1 |
| NaOAc | Glucose | 0-4 | 27 ± 3 | 46 ± 2 | 1.0 ± 0.0 | 1.7 ± 0.0 | 7 ± 1 |
| (pH = 3) | | 4-12 | 29 ± 0 | 49 ± 1 | 0.5 ± 0.0 | 1.4 ± 0.1 | 8 ± 0 |
| | | 12-50 | 31 ± 2 | 50 ± 3 | 0.5 ± 0.0 | 1.4 ± 0.1 | 9 ± 1 |
| | Oxalic acid | 0-4 | 23 ± 3 | 39 ± 2 | 0.8 ± 0.1 | 1.9 ± 0.2 | 6 ± 1 |
| | | 4-12 | 26 ± 3 | 49 ± 3 | 0.7 ± 0.0 | 1.7 ± 0.3 | 6 ± 1 |
| | | 12-50 | 29 ± 2 | 51 ± 3 | 0.5 ± 0.1 | 1.5 ± 0.1 | 8 ± 1 |
| | Acetic acid | 0-4 | 37 ± 2 | 55 ± 0 | 0.6 ± 0.0 | 1.4 ± 0.1 | 10 ± 1 |
| | | 4-12 | 32 ± 0 | 54 ± 2 | 0.5 ± 0.1 | 1.3 ± 0.2 | 9 ± 1 |
| | | 12-50 | 30 ± 3 | 53 ± 1 | 0.5 ± 0.1 | 1.4 ± 0.1 | 8 ± 1 |
| | Control | 0-4 | 33 ± 1 | 55 ± 2 | 0.5 ± 0.0 | 1.4 ± 0.0 | 9 ± 0 |
| | | 4-12 | 32 ± 3 | 55 ± 2 | 0.5 ± 0.0 | 1.3 ± 0.0 | 9 ± 0 |
| | | 12-50 | 31 ± 2 | 54 ± 3 | 0.5 ± 0.0 | 1.3 ± 0.0 | 8 ± 1 |
| AAO | Glucose | 0-4 | 45 ± 3 | 34 ± 0 | 9 ± 2 | 0.6 ± 0.1 | 60 ± 5 |
| (pH = 3) | | 4-12 | 45 ± 5 | 34 ± 1 | 10 ± 1 | 0.6 ± 0.0 | 57 ± 6 |
| | | 13-50 | 45 ± 3 | 35 ± 0 | 11 ± 0 | 0.6 ± 0.1 | 60 ± 5 |
| | Oxalic acid | 0-4 | 51 ± 4 | 36 ± 3 | 8 ± 1 | 0.6 ± 0.5 | 46 ± 6 |
| | | 4-12 | 47 ± 7 | 35 ± 1 | 8 ± 0 | 0.6 ± 0.0 | 55 ± 2 |
| | | 13-50 | 45 ± 1 | 35 ± 2 | 10 ± 1 | 0.6 ± 0.0 | 59 ± 2 |
| | Acetic acid | 0-4 | 47 ± 5 | 35 ± 2 | 11 ± 1 | 0.7 ± 0.0 | 58 ± 6 |
| | | 4-12 | 45 ± 3 | 33 ± 0 | 10 ± 0 | 0.6 ± 0.0 | 58 ± 7 |
| | | 13-50 | 47 ± 4 | 34 ± 1 | 11 ± 0 | 0.6 ± 0.1 | 56 ± 6 |
| | Control | 0-4 | 46 ± 0 | 36 ± 0 | 11 ± 0 | 0.6 ± 0.0 | 61 ± 1 |
| | | 4-12 | 45 ± 1 | 35 ± 1 | 10 ± 0 | 0.6 ± 0.1 | 60 ± 1 |
| | | 13-50 | 46 ± 3 | 35 ± 2 | 10 ± 0 | 0.6 ± 0.1 | 60 ± 0 |

67

**Table S-5: Alpha diversity indices (< 97%) based on pyrosequencing data of root, intermediate and bulk zones for each exudate treatment**

| Treatment | Control | | | Glucose | | | Acetate | | | Oxalate | | |
|---|---|---|---|---|---|---|---|---|---|---|---|---|
| Distance to root (mm) | 0-4 | 5-12 | 13-50 | 0-4 | 5-12 | 13-50 | 0-4 | 5-12 | 13-50 | 0-4 | 5-12 | 13-50 |
| Diversity indices: | | | | | | | | | | | | |
| OTUs | 383 | 357 | 386 | 393 | 417 | 325 | 296 | 379 | 355 | 254 | 384 | 437 |
| PD (whole tree)[1] | 24 | 23 | 23 | 22 | 26 | 20 | 17 | 21 | 22 | 15 | 24 | 27 |
| CHAO 1[2] | 749 | 633 | 726 | 676 | 690 | 568 | 484 | 593 | 632 | 455 | 672 | 705 |
| Shannon[3] | 7 | 7 | 8 | 8 | 8 | 7 | 7 | 8 | 7 | 6 | 7 | 8 |
| Simpson[4] | 0.97 | 0.98 | 0.99 | 0.99 | 0.99 | 0.94 | 0.98 | 0.99 | 0.97 | 0.6 | 0.98 | 0.99 |

[1] (Faith and Baker, 2007)
[2] (Chao, 1984)
[3] (Shannon, 1948)
[4] (Simpson, 1949)

**Table S-6: pH, pore water concentrations of mobilized organic C and dissolved metal cations in the root zone (0-4 mm) (mean ± standard error, n = 2) of silt loam**

| Treatment | pH[#] | $C_{org}$ | Al | Mn | Ca | Fe |
|---|---|---|---|---|---|---|
| | | mg $l^{-1}$ | | $\mu$M | | |
| Glucose | 5.2 ± 0.3 | 1.9 ± 0.9 | 35 ± 0 | 6 ± 3 | 400 ± 100 | 8 ± 2 |
| Acetic acid | 6.4 ± 0.2 | 5 ± 2 | 40± 30 | 6 ± 0 | 270 ± 70 | 80 ± 20 |
| Oxalic acid | 7.2 ± 0.3 | 36 ± 1 | 540 ± 80 | 6 ± 0 | 130 ± 20 | 250 ± 70 |
| Control | 5.7 ± 0.2 | 2.1 ± 0.7 | 52 ± 2 | 3 ± 0 | 350 ± 20 | 20 ± 10 |

[#] in 0.01M $CaCl_2$

70

**Table S-7: C 1s NEXAFS peak assignments**

| C functional group | Photon energy [eV] |
|---|---|
| Aromatic C | 284-285.5 |
| Phenolic C | 286.5–287 |
| Aliphatic C | 287.1–287.8 |
| Carboxyl C/ Amide C | 288.0–288.8 |
| O-alkyl C | 289-289.5 |
| Carbonyl C | 290-290.5 |

References: (Cody et al., 2011, 1998; Kleber et al., 2011; Solomon et al., 2005)

71
72

**Table S-8: Energies used to map the concentration of each element using difference maps**

| Absorption edge | Pre-edge (eV) | Peak (eV) |
|---|---|---|
| C 1s | 280 | 295 |
| N 1s | 398 | 407 |
| O 1s | 528 | 545 |
| Ca 2p | 340 | 349.3 |
| Mn 2p | 636 | 640 |
| Fe 2p | 700 | 709.5 |

**Table S-9: Average $\delta^{13}C$ values and the calculated percentage of exudate-derived C for organic C in the pore water samples analyzed by NanoSIMS (mean ± standard error)**

| Treatment | $\delta^{13}C$ (‰) | % exudate-derived C | n (number of regions analyzed) |
|---|---|---|---|
| Glucose | 40 ± 9 | 0.4 | 8 |
| Acetic acid | 220 ± 30 | 2.2 | 9 |
| Oxalic acid | 65 ± 4 | 0.7 | 10 |

75
76

**Table S-10: Metal mobilization 1 and 48 hours after oxalic acid and glucose additions to both soils[&]**

| Soil | Exudate treatment | Incubation time | Fe | Al |
|---|---|---|---|---|
| | | hours | mg $L^{-1}$ | mg $L^{-1}$ |
| Grassland (silt-loam) | Glucose | 1 | 0.04(0.01) | 0.22(0.04) |
| | Oxalic Acid | | 29(3) | 130(10) |
| | Control (DI $H_2O$) | | 0.009(0.003) | 0.20(0.04) |
| Forest (clay) | Glucose | | n.d. | 0.16(0.03) |
| | Oxalic Acid | | 16(1) | 171(3) |
| | Control (DI H2O) | | 0.017(0.004) | 0.27(0.06) |
| Grassland (silt-loam) | Glucose | 48 | 0.05(0.02) | 0.17(0.05) |
| | Oxalic Acid | | 14(3) | 79(6) |
| | Control (DI $H_2O$) | | 0.017(0.005) | 0.06(0.01) |
| Forest (clay) | Glucose | | 0.32(0.03) | 0.4(0.3) |
| | Oxalic Acid | | 2.4(0.2) | 33(3) |
| | Control (DI $H_2O$) | | 0.2(0.1) | 0.4(0.1) |

[&] Two g of air-dried soil was given to serum vials, amended with 2 ml of the exudate solution used for the artificial root experiments, and the vials were capped. After 1 or 48 hours, pore water samples were extracted and Fe and Al concentrations were determined as described in the methods section of the main article.

77

## 2. Figure captions

Figure S-1: Schematic of the artificial root microcosms

Figure S-2: $O_2$ concentrations as a function of distance to the root in clay soil. Points represent mean ± standard error of the mean (n = 2). Asterisks denote locations with mean $O_2$ concentrations significantly lower than the control determined (one-way ANOVA, Tukey's *ad-hoc* HSD test, $p < 0.05$). Solid lines represent model fits used to calculate microbial $O_2$ consumption based on Fick's first law of diffusion (Højberg and Sørensen, 1993). The inset shows volume-specific rates of $O_2$ consumption in the rhizosphere for each exudate treatment. See Table S-2 and section 6.1 for details on fitting parameters and rate calculations.

Figure S-3: Microbial community response to exudate additions. (a) Bacterial and archaeal unweighted Unifrac distances (a measure of phylogenetic dissimilarity between communities) as influenced by treatment and distance to the root. Both replicate treatments are shown. (b) Average relative abundances of dominant phyla as a function of treatment in the root zone (distance to root = 0-4 mm). Asterisks denote significant differences compared to the control (one-way ANOVA, Tukey's *ad-hoc* HSD test, $p < 0.05$).

Figure S-4: Average LDPI mass spectra of organic C present in the pore water (black line) shown with the laser background for comparison (red line).

Figure S-5: Averaged carbon K-edge NEXAFS spectra of pore water C recovered from clay-rich forest soil exposed to the respective exudate treatments.

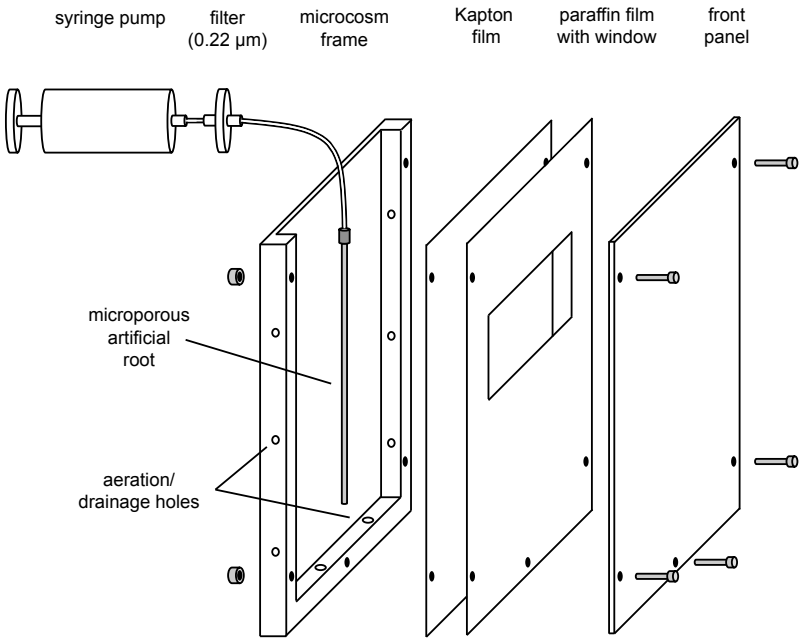
syringe pump
filter
(0.22 µm)
microcosm
frame
Kapton
film
paraffin film
with window
front
panel
microporous
artificial
root
aeration/
drainage holes

**Figure S-1**

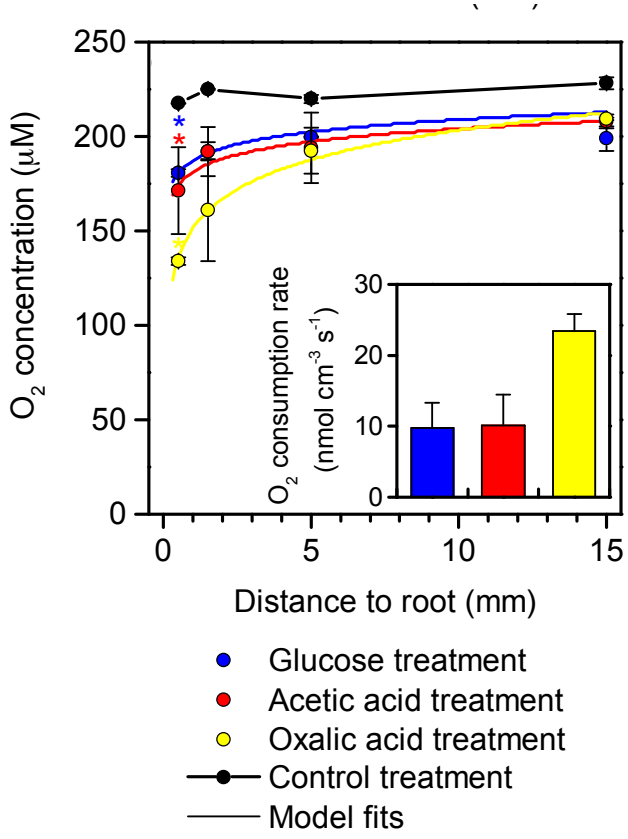


102

103 **Figure S-2**

104

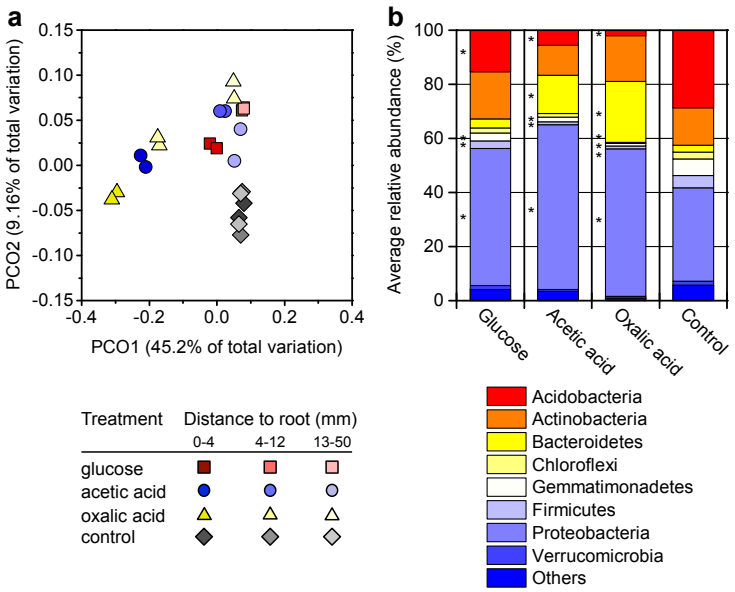
a
b
PCO2 (9.16% of total variation)
PCO1 (45.2% of total variation)
Average relative abundance (%)
Glucose
Acetic acid
Oxalic acid
Control
Treatment
Distance to root (mm)
0-4
4-12
13-50
glucose
acetic acid
oxalic acid
control
Acidobacteria
Actinobacteria
Bacteroidetes
Chloroflexi
Gemmatimonadetes
Firmicutes
Proteobacteria
Verrucomicrobia
Others

**Figure S-3**

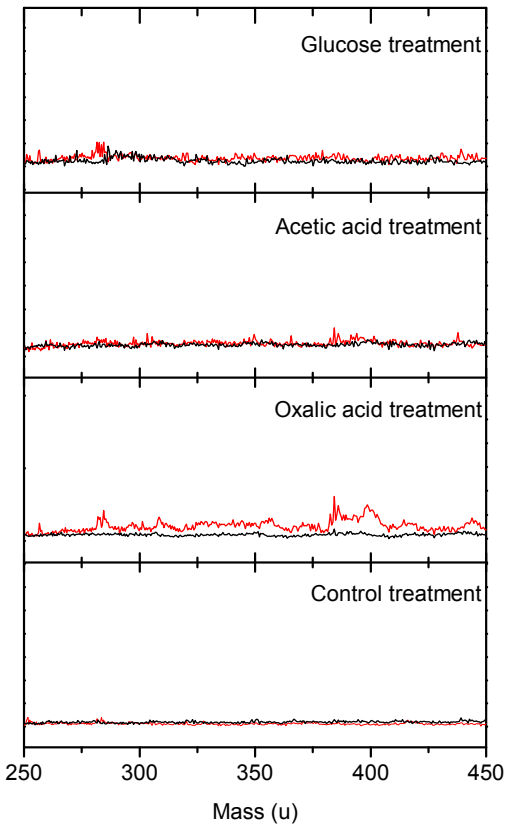
Glucose treatment
Acetic acid treatment
Oxalic acid treatment
Control treatment
250
300
350
400
450
Mass (u)

**Figure S-4**

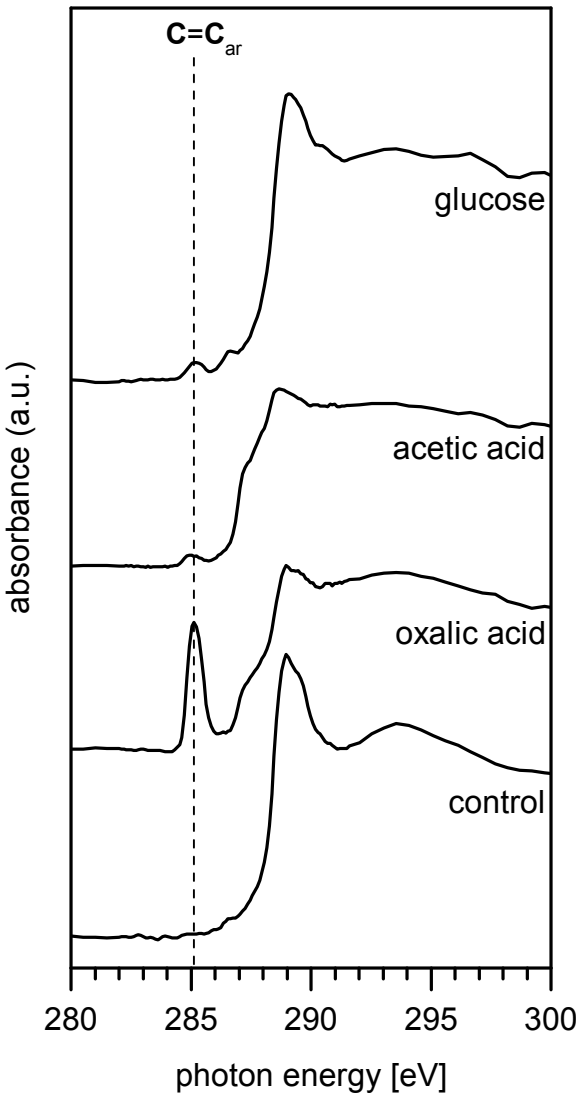
C=C ar
glucose
acetic acid
oxalic acid
control
absorbance (a.u.)
280
285
290
295
300
photon energy [eV]

**Figure S-5**

115

116 **3. Soil characteristics and handling**

117 **3.1 Field sampling**

118 To test the universal nature of the rhizosphere effect, two soils were chosen to represent two
119 important biomes, forests and grasslands. A clay loam (Humic Dystrudept) under coniferous
120 forest (H.J. Andrews Experimental Forest, Oregon, USA) and a medium-textured silt loam
121 (Typic Haploxeroll) under cultivation with wheat (Hermiston Agricultural Research & Extension
122 Center, Oregon, USA) were sampled in spring 2011. At both sites, volumetric (undisturbed soil
123 cores) and bulk (homogenized) samples were collected from surface horizons ($A_p$ and $A_h$,
124 respectively) and stored moist at 4˚C until further use. Core samples were used to determine bulk
125 density and field capacity, whereas mixed samples were split into two halves. One half served
126 for general sample characterization in the laboratory, such as water and ash content, pH,
127 elemental composition and mineralogy. The other half was used for experiments. Both soils
128 widely differed in their physical and chemical characteristics (Table S-1).

129 **4. Experimental approach**

130 **4.1 Exudate solutions**

131 Exudate solutions were prepared in MilliQ water containing inorganic nutrients (330 $\mu$M KCl,
132 70 $\mu$M $KH_2PO_4$ and 70 $\mu$M $MgSO_4$) for osmoregulation. The concentrations of each exudate
133 solution were normalized on a C-basis such that 15 $\mu$mol C $cm^{-2}$ $d^{-1}$ were provided. Supplied at a
134 rate of 1 ml $d^{-1}$, exudate C supplied through the root amounted to 4.2 mmol of C per microcosm
135 over the course of the 35d incubation period. Given a C content of 1.4 and 1.5% for silt-loam and
136 clay soil, respectively, and assuming that approximately 10 g of soil surrounding the root are
137 affected, exudate C additions amount to approximately 36 and 34% of total soil C at the end of
138 the experiment (for silt-loam and clay soil, respectively). The pH of D-glucose, acetic acid, and
139 oxalic acid solutions was then buffered to pH 7, 4.75 and 4.27, respectively, using 1M NaOH
140 and filter-sterilized (0.22 $\mu$m) before transfer into the syringe pump. Control microcosms
141 received filter-sterilized (0.22 $\mu$m) inorganic nutrient solution only.

142 **4.2 Microcosm design**

143 Fig. S-1 shows an exploded diagram of the microcosms designed for delivery of root
144 exudate solutions. Each microcosm consisted of a 15 × 12 × 1 cm clear acrylic frame with a 14 ×

10 × 0.8 cm opening, and an acrylic front panel was attached for protection. Fig. S-1 further shows the position of the microporous cylindrical rhizon samplers (length = 10 cm, diameter = 2.5 mm) serving as artificial root to deliver the exudate solutions (Soilmoisture Equipment Corp, USA). The removable front panel and protective, gas diffusion-limiting Kapton film cover allowed for $O_2$ microsensor measurements without disturbing the system. Aeration holes in the frame were filled with glass wool and allowed for steady air circulation through the soil.

### 4.3 Incubations

Soils were air-dried just enough to facilitate sieving (2-mm sieve). Soils were subsequently homogenized, wetted to 75% field capacity with MilliQ water, and pre-incubated at constant moisture in the dark for 7 d at 25˚C before the experiment. After preincubation, soils were carefully packed into microcosm frames containing the artificial root, thereby aiming to reproduce the field bulk density values of 1.05 (clay) and 1.24 (silty-loam) g $m^{-1}$ . Soils were then covered using Kapton and paraffin films. Both films were firmly sealed to the edge of the frame using double-sided Scotch tape. Microcosms were wrapped in ultraclean aluminum foil and transferred to the environmental chamber where they were connected to the syringe pump.

4.4

## 5. Analysis of physical-chemical gradients across individual zones (root, intermediate, and bulk)

### 5.1 $O_2$ profiling

To measure oxygen profiles without disturbing the soil, microcosms were placed on the back panel and the front plate of the microcosm was carefully removed while the soil was held in place by both Kapton and paraffin films. At the desired sampling location, a droplet of agar medium was pipetted on the transparant Kapton film and the film underneath was punctured using a sterile syringe needle. The tip of the microsensor, mounted on a micromanipulator (MM33-2, Unisense, Denmark) and connected to a picoamperemeter (PA-2000, Unisense, Denmark), was then slowly lowered through the agar medium covering the hole in the Kapton film into the soil. In this setup, the agar medium served as a sealant to slow down oxygen diffusion through the hole. To establish oxygen concentration profiles, six replicate measurements were conducted at distances of 0.5, 1, 5 and 15 mm from the root in each microcosm. For consistency, oxygen concentrations in the soil were always recorded at the position closest to the root, i.e., 4 mm from the surface of the soil facing the front plate. After completion, front plates were reattached and microcosms were transferred to an anaerobic glove box. Oxygen profiles for the clay loam are shown in Fig. S-2.

Diffusion model parameters and $O_2$ consumption calculations:

Specific oxygen consumption rates in the soil surrounding the artificial root were calculated as described in Nielsen et al. (1990) and Højberg and Sørensen (1995).

First, to describe the oxygen profile an equation of the form

$$C(r) = A_1 \ln(r) + A_2 \quad (2)$$

where C(r) is the concentration of oxygen at a distance r from the root surface and $A_1$ and $A_2$ are constants resulting from the integration procedure, was derived from Fick's second law of diffusion applied to a cylindrical root system assumed to be at steady state. Equation 2 was then fitted to the measured data using the damped least-squares (DLS) method (see Table S-2 for fit results).

Second, for the equations describing the fitted curves (Table S-2), a first derivative $\frac{\partial C(r)}{\partial r}$ was obtained to calculate oxygen diffusion fluxes for each treatment. The system was considered to be radially symmetric around the root, and diffusion fluxes of oxygen were determined from Fick's first law of diffusion applied to a cylinder

$$J(r) = -n\, D_s\, \frac{\partial C(r)}{\partial r} \quad (3)$$

where $J(r)$ is the diffusive flux per unit of surface area at a distance r from the center of the root axis, $n$ and $D_s$ are the porosity and the diffusion coefficient of the respective soils. Effective diffusion coefficients ($D_e$) for both soils were estimated based on porosity and volumentric water contents (Aachib et al., 2004), with $D_s$ values of 1.43 × 106 $m^2$ $s^{-1}$ for silt-loam and 0.81 × 106 $m^2$ $s^{-1}$ for clay.

Finally, specific oxygen consumption rates were calculated by multiplying the diffusive flux (mass per surface area per time) with the surface of the cylinder ($2\pi rh$) and dividing by the volume ($\pi r2h$) of the root cylinder. The radius of the artificial root was 0.125 cm and rates were reported in units of nmol $cm^{-3}$ $s^{-1}$.

### 5.2 Microcosm sampling

After completion of the oxygen measurements, microcosms were transferred into an anaerobic glove box where parafilm and Kapton film covers were removed. Soil from three zones surrounding the artificial root (0-4, 5-12, and 13-50 mm) was excised. Excised samples were thoroughly mixed and subsamples were processed directly (pH measurements and sequential extractions), air-dried (elemental analysis), or stored at -80 ˚C until further processing (DNA/RNA extraction).

### 5.3 Sequential extraction of reactive mineral phases

In the anaerobic glove box, an aliquot of moist soil equivalent to 1g of oven-dry soil was combined with 40 ml of extractant solution in a 50 ml polypropylene centrifuge tube, agitated in the dark using a reciprocal shaker, and centrifuged (Table S-3). After centrifugation, the supernatant was removed, filtered through 0.22 $\mu$m syringe filters, stabilized in 1% high-purity $HNO_3$, and stored at 4˚C before ICP-MS analysis. Prior to the next extraction step, the solid residue remaining in the centrifuge tube was washed twice (by adding 20 mL of MilliQ water, shaking vigorously by hand, then centrifuging at 17,000 x g for 15 min) to remove entrained

solution and minimize interaction between the different extracting solutions. All solutions were purged of oxygen and equilibrated in the glove box prior to use. Absolute concentrations determined by ICP-MS are reported in Tables S-4.

### 5.4 DNA/RNA extractions and pyrosequencing

DNA and RNA were extracted from soil samples using a Mobio RNA Powersoil kit in combination with a Mobio RNA Powersoil DNA elution accessory kit as per manufacturer's protocol. Between 1.8 and 2 g of soil was transferred to a bead beating specific 15mL tube. Samples were homogenized using a FastPrep-24 (MP Biomedicals, California, USA) run at a speed of 4 m/s for 3 bursts of 30 seconds. RNA and DNA were eluted in final volumes of 40ul of RNAse free water. RNA and DNA were quantified using a Nanodrop 2000 (Thermo Scientific, Willmington, USA). Samples were stored at -80 ˚C until further processing.

Pyrotag sequencing was done at Research and Testing Laboratory (Texas, USA) using a Roche Genome sequence FLX+ 454 sequencer. Sequencing targeted identification of prokaryotic 16S ribosomal sequences and fungal ribosomal sequences (ITS region for rDNA and LSU region for rRNA). Prokaryotic data used primers 926F and 1392R for both RNA and DNA samples. Fungal data was obtained using primers ITS1F and ITS4R for DNA samples and primers XX for RNA samples. All samples were sequenced to a theoretical depth of at least 3000 sequences per sample. RNA samples were converted to cDNA prior to analysis. Each sample was amended with a unique 8 bp 'tag' to be used for post sequencing separation.

Pyrotag sequence data were denoised (Edgar et al. 2010) and chimera checked (Edgar et al. 2011) before analysis in QIIME (Caporaso et al., 2010). Representative sequences for individually defined OTUs based on >97% similarity were used for all analyses and OTUs with only one representative were removed (Edgar, 2010) and taxonomy of each was determined using uclust (McDonald et al., 2012; Wang et al., 2007). Sequences were aligned and a phylogentic tree was created (Price et al., 2010) and used to calculate alpha and beta diversity indices. Alpha diversity indices; including Simpson, Shannon and chao 1; were calculated for each sample (Table S-5). Beta diversity analyses, consisting of principle coordinates analysis calculated from weighted UniFrac data, were used to show similarity of samples. In all cases, sequencing effort for each sample was standardised based on rarefication and based on at least 1000 sequences each.

### 5.5 Isotope ratio mass spectrometry ($\delta^{13}C$ and total C) analysis

Total C and $\delta^{13}C$ enrichment of soil collected from individual zones was determined using a LECO (St. Joseph, MI, USA) isotope ratio mass spectrometer (IRMS) at the Oregon State University Stable Isotope Research Unit, and were referenced to Vienna Pee Dee Belemnite (VPDB). $\delta^{13}C$ values were calculated as follows:

$$\delta^a X = \left(\frac{R_m}{R_{STD}} - 1\right) \times 1000 \ [‰]$$

where $R_m$ is the isotopic ratio of the sample and $R_{STD}$ that of the reference standard.

## 6. Characterization of pore water C

### 6.1 UV/vis spectroscopy

Due to the low sample volume (100-200 $\mu$L), organic carbon concentrations in the pore water were calculated from their absorbance at 450 nm (Yang et al., 2001). Visible spectra of pore water samples were obtained using a UV/vis spectrophotometer, and concentrations were calculated based on Beer's law and a extinction coefficient ($\varepsilon_{450}$) of $5.75 \times 10^{-3}$ l $cm^{-1}$ $mg^{-1}$ organic C. $\varepsilon_{450}$ was determined based on the absorbance of a series of DOC standard solutions with organic C concentrations verified using a Shimadzu TOC 5000. Organic C concentrations in the pore water samples are shown in Table S-6.

### 6.2 Inductively coupled plasma mass spectrometry (ICP-MS) analysis of inorganic constituents

Al, Si, Mn, Ca and Fe concentrations (Table S-4) in acidified (1% $HNO_3$) pore water samples were measured using a Perkin Elmer SCIEX Elan DRC II Inductively Coupled Plasma Mass Spectrometer (ICP-MS).

### 6.3 Laser desorption synchrotron ionization (LDSI) mass spectrometry

Laser Desorption Synchrotron Ionization (LDSI) mass spectrometry was performed on a modified time-of-flight secondary ion mass spectrometer (TOF.SIMS V; IonTOF, Germany) coupled to a synchrotron VUV light port at beamline 9.0.2 of the Advanced Light Source, Lawrence Berkeley National Laboratory (Kostko et al., 2011; Takahashi et al., 2011). Prior to analysis, 2 $\mu$L aliquots of pore water sample were pipetted on silicon substrates (Wafer World,

Inc., USA) and air-died. The desorption laser was calibrated to emit 8.5 ns pulses focused to a spot diameter of ~30 $\mu$m, and its power was reduced until no laser-induced fragmentation could be detected in the background (~0.7 MW $cm^{-2}$) while achieving sufficient desorption efficiency. The UV energy was tuned to 10.5 eV to specifically target aromatic fragments with low ionization thresholds (Hanley and Zimmermann, 2009). Using this setup, the sample was raster-scanned at 2 mm $s^{-1}$ over a 500 x 500 $\mu$m area to minimize the impact of the laser. Mass spectra were binned and normalized to the highest signal intensity. Averaged mass spectra of pore water extracted from silt-loam are displayed with their respective laser background from 250-450 u (Fig. S-3).

### 6.4 Scanning transmission X-ray absorption microscopy/near-edge X-ray absorption fine structure (STXM/NEXAFS)

Stack images were aligned via a spatial cross-correlation analysis, clean areas of the $Si_3N_4$ membrane were used to normalize the transmission signal obtained from analyzed ROIs, and NEXAFS spectra were extracted from groups of pixels of individual organic colloids using the aXis 2000 software package (Hitchcock, 2009). Extracted C NEXAFS spectra were normalized using the Athena software package for X-ray absorption spectroscopy (Ravel and Newville, 2005). Edge step normalization was performed using set $E_0$ values of 290 eV across the full recorded range (278–330 for C 1s). Peak assignments can be found in the Table S-7.

The relative abundance of C, Ca, N, O, Mn and Fe species was mapped by calculating the difference between two images converted to optical density maps, one measured above the respective edge and one below the respective absorption edge. The energies used are given in Table S-8.

### 6.5 High spatial resolution secondary ion mass spectrometry (NanoSIMS)

To determine whether organic colloids in the pore water were derived from native organic matter in the soil (with a $\delta^{13}C$ signature of ~0 ‰) or from the isotopically-labeled exudate C provided ($\delta^{13}C$ ~ 8800 ‰) to the soil, isotopic images were acquired on a NanoSIMS 50 (Cameca, Gennevilliers, France) at Lawrence Livermore National Laboratory. This instrument allows the simultaneous imaging of five isotopes with high spatial resolution (up to 50 nm) and high mass resolution. For this study, electron multiplier (EM) detectors were positioned to collect $^{12}C^-$, $^{13}C^-$, $^{12}C^{14}N^-$, and $^{12}C^{15}N^-$. Due to the poor yield of $N^-$, nitrogen was detected as the molecular ion $CN^-$. The secondary ion mass spectrometer was tuned for a mass resolving power (defined as $M/\Delta M$,

where $M$ designates the mass and $\Delta M$ is the mass difference between the mass of interest and the isobaric interference) of > 6800 in order to resolve isobaric interferences.

Ion images of the ROIs previously imaged by STXM were generated with a 1.5 pA $Cs^+$ primary beam, focused to a spot size of ~100 nm, and stepped over the sample in a 256 x 256 pixel raster. Dwell time was 1 ms/pixel, and raster size was 10 x 10 $\mu$m. Secondary ions were detected in simultaneous collection mode by pulse counting to generate 60–180 serial quantitative secondary ion images (or 'layers').

NanoSIMS image data were processed as quantitative isotopic ratio images using the LIMAGE software package developed by L. Nittler (Carnegie Institution of Washing- ton), and were corrected for effects of quasi-simultaneous arrival (QSA), detector dead-time and image shift from layer to layer (due to drift in the location of the ion beam from frame to frame). Data planes collected before sputtering equilibrium was achieved (typically 5–10) were discarded. The isotopic composition ($\delta^{13}C$) of each ROI was calculated by averaging over all replicate layers where C isotopes were at sputtering equilibrium. Repeated NanoSIMS analyses of a *Bacillus subtilis* spore preparation were used as a reference standard for the C and N isotopic measurements ($\delta^{13}C$ = -14.4‰) (Kreuzer-Martin and Jarman, 2007). Isotopic enrichment of standards was independently determined at the University of Utah and used to normalize sample analysis as described previously by (Finzi-Hart et al., 2009). Mean $\delta^{13}C$ of pore water C regions previously analyzed by STXM are given in Table S-9.

## 7. Bibliography


Aachib, M., Mbonimpa, M., Aubertin, M., 2004. Measurement and prediction of the oxygen diffusion coefficient in unsaturated media, with applications to soil covers. Water, air, and soil pollution 156, 163–193.

Caporaso, J.G., Kuczynski, J., Stombaugh, J., Bittinger, K., Bushman, F.D., Costello, E.K., Fierer, N., Peña, A.G., Goodrich, J.K., Gordon, J.I., Huttley, G.A., Kelley, S.T., Knights, D., Koenig, J.E., Ley, R.E., Lozupone, C.A., McDonald, D., Muegge, B.D., Pirrung, M., Reeder, J., Sevinsky, J.R., Turnbaugh, P.J., Walters, W.A., Widmann, J., Yatsunenko, T., Zaneveld, J., Knight, R., 2010. QIIME allows analysis of high-throughput community sequencing data. Nat Meth 7, 335–336.

Chao, A., 1984. Nonparametric Estimation of the Number of Classes in a Population. Scandinavian Journal of Statistics 11, 265–270.

Edgar, R.C., 2010. Search and clustering orders of magnitude faster than BLAST. Bioinformatics 26, 2460–2461.

Faith, D.P., Baker, A.M., 2007. Phylogenetic diversity (PD) and biodiversity conservation: some bioinformatics challenges. Evol Bioinform Online 2, 121–128.

Finzi-Hart, J.A., Pett-Ridge, J., Weber, P.K., Popa, R., Fallon, S.J., Gunderson, T., Hutcheon, I.D., Nealson, K.H., Capone, D.G., 2009. Fixation and fate of C and N in the cyanobacterium Trichodesmium using nanometer-scale secondary ion mass spectrometry. PNAS 106, 6345–6350.

Hanley, L., Zimmermann, R., 2009. Light and Molecular Ions: The Emergence of Vacuum UV Single-Photon Ionization in MS. Anal. Chem. 81, 4174–4182.

Hitchcock, A.P., 2009. aXis2000 software package. Available from: <http://unicorn.mcmaster.ca/aXis2000.html/>.

Kostko, O., Takahashi, L.K., Ahmed, M., 2011. Desorption dynamics, internal energies, and imaging of organic molecules from surfaces with laser desorption and vacuum ultraviolet (VUV) photoionization. Chem Asian J 6, 3066–3076.

Kreuzer-Martin, H.W., Jarman, K.H., 2007. Stable Isotope Ratios and Forensic Analysis of Microorganisms. Appl Environ Microbiol 73, 3896–3908.

McDonald, D., Price, M.N., Goodrich, J., Nawrocki, E.P., DeSantis, T.Z., Probst, A., Andersen, G.L., Knight, R., Hugenholtz, P., 2012. An improved Greengenes taxonomy with explicit

362 ranks for ecological and evolutionary analyses of bacteria and archaea. ISME J 6, 610–
363 618.
364 Price, M.N., Dehal, P.S., Arkin, A.P., 2010. FastTree 2 – Approximately Maximum-Likelihood
365 Trees for Large Alignments. PLoS ONE 5, e9490.
366 Ravel, B., Newville, M., 2005. ATHENA, ARTEMIS, HEPHAESTUS: data analysis for X-ray
367 absorption spectroscopy using IFEFFIT. J Synchrotron Radiat 12, 537–541.
368 Shannon, C.E., 1948. A mathematical theory of communication. The Bell System Technical
369 Journal 27,, 623–656.
370 Simpson, E.H., 1949. Measurement of diversity. Nature 163, 688.
371 Takahashi, L.K., Zhou, J., Kostko, O., Golan, A., Leone, S.R., Ahmed, M., 2011. Vacuum-
372 ultraviolet photoionization and mass spectrometric characterization of lignin monomers
373 coniferyl and sinapyl alcohols. J Phys Chem A 115, 3279–3290.
374 Wang, Q., Garrity, G.M., Tiedje, J.M., Cole, J.R., 2007. Naïve Bayesian Classifier for Rapid
375 Assignment of rRNA Sequences into the New Bacterial Taxonomy. Appl. Environ.
376 Microbiol. 73, 5261–5267.
377 Yang, Y., Ratte, D., Smets, B.F., Pignatello, J.J., Grasso, D., 2001. Mobilization of soil organic
378 matter by complexing agents and implications for polycyclic aromatic hydrocarbon
379 desorption. Chemosphere 43, 1013–1021.
380